

Implicit Folding Simulation of Ultrathin Shells Using Refined One-Dimensional Finite Elements

*Original*

Implicit Folding Simulation of Ultrathin Shells Using Refined One-Dimensional Finite Elements / Augello, R., Pellegrino, S.. - In: AIAA JOURNAL. - ISSN 0001-1452. - 63:12(2025), pp. 5405-5415. [10.2514/1.j065448]

*Availability:*

This version is available at: 11583/3008180 since: 2026-03-04T12:59:13Z

*Publisher:*

AIAA International

*Published*

DOI:10.2514/1.j065448

*Terms of use:*

This article is made available under terms and conditions as specified in the corresponding bibliographic description in the repository

*Publisher copyright*

AIAA preprint/submitted version e/o postprint/Author's Accepted Manuscript

© AIAA. Implicit Folding Simulation of Ultrathin Shells Using Refined One-Dimensional Finite Elements / Augello, Riccardo; Pellegrino, Sergio published in : AIAA JOURNAL, 2025, 63, 12, 5405-5415, <http://dx.doi.org/10.2514/1.j065448>.

(Article begins on next page)

# Implicit Folding Simulation of Ultrathin Shells Using Refined One Dimensional Finite Elements

Riccardo Augello\*

*California Institute of Technology, Pasadena, CA, 91125<sup>‡</sup>*

Sergio Pellegrino<sup>†</sup>

*California Institute of Technology, Pasadena, CA, 91125*

The focus of this study is the numerical simulation of the folding of ultra-thin shells, focusing on slender deployable longerons. The proposed solution leverages the finite element method, specifically within the framework of the Carrera Unified Formulation, to develop one-dimensional finite elements with enhanced three-dimensional capabilities. Refined one-dimensional beam finite elements are used to model the longerons, and the three-dimensional displacement field is computed as a general expansion of the nodal displacements along the axis. The folding of these deployable structures is simulated with an implicit approach, and quasi-static simulation is performed. Moreover, a novel node-to-surface contact is introduced, where nonlinear springs act upon predefined node-pairs. Simulations of a 400 mm-long longeron are conducted to fine-tune the parameters of the nonlinear spring stiffness. A deployable structure comprising two 400 mm-long longerons connected by transverse straight battens is analyzed. The results are compared with reference results obtained with the Abaqus software, revealing a noteworthy degree of agreement. The proposed method is also employed to simulate the folding of longer strips (1 m and 5 m in length), where elements are not strictly constrained by aspect ratios, and it efficiently handles these structures.

## Nomenclature

$b_l$	=	linear differential operator
$b_{nl}$	=	nonlinear differential operator
$\mathbf{C}$	=	stiffness matrix for linear elastic material
$F_\tau$	=	expansion functions along thickness coordinate $z$

---

\*Corresponding author. <sup>‡</sup>Visitor Postdoc, Graduate Aerospace Laboratories, MC 105-50. California Institute of Technology, Pasadena, CA, 91125. E-mail: raugello@caltech.edu

Currently: Postdoc, Politecnico di Torino, Torino, Italy, 10129. E-mail: riccardo.augello@polito.it.

<sup>†</sup>Joyce and Kent Kresa Professor of Aerospace and Civil Engineering; Jet Propulsion Laboratory Senior Research Scientist; Co-Director, Space-Based Solar Power Project, Graduate Aerospace Laboratories, MC 105-50. California Institute of Technology, Pasadena, CA, 91125. AIAA Fellow. E-mail: sergiop@caltech.edu

$\mathbf{K}_S^{ij\tau s}$	=	fundamental nucleus of secant stiffness matrix
$\mathbf{K}_T^{ij\tau s}$	=	fundamental nucleus of tangent stiffness matrix
$\mathbf{L}_{ine}$	=	work of inertial loads
$\mathbf{L}_{ext}$	=	work of external loads
$\mathbf{L}_{int}$	=	strain energy
$M$	=	number of terms in expansion in cross-section plane
$N_i$	=	shape function
$N_n$	=	number of finite element nodes per element
$\mathbf{u}_\tau, \mathbf{u}_{\tau i}$	=	generalized displacement vector and finite element nodal parameters
$\delta$	=	variation
$\epsilon$	=	strain vector
$\sigma$	=	stress vector

## I. Introduction

The recent miniaturization of electronics in space systems has led to significant reductions in size and cost of spacecraft system, but large aperture components, such as telescopes, antennas, and solar arrays, must unavoidably maintain a substantial size. To address the requirement of low cost satellites that accommodate sizable apertures, the demand for deployable structures has been increasing. Structures that are elastically coiled and can be unfurled to assume a rod-like or surface-like shape, releasing the stored energy during deployment, have found numerous applications [? ? ].

The most prevalent type of such structures is based on tape springs, i.e. thin elastic strips with circular arc cross-section. Tape springs have been adopted for a large number of applications, including high-resolution deployable telescopes [? ], collapsible rib-tensioned mesh reflectors [? ] and rigid-panel solar arrays [? ]. The behavior of a metallic tape spring subject to opposite-sense bending was first studied by Wuest [? ]. Later, Mansfield studied the large-deflection torsional and flexural behavior of tape springs [? ]. The deployment dynamics of tape springs were studied by Seffen and Pellegrino [? ]. Recently, carbon fibre reinforced plastic tape springs were developed in order to achieve higher stiffness to mass ratio [? ].

The Triangular Rollable And Collapsible (TRAC) boom, conceived by Murphey and Banik [? ] at the Air Force Research Laboratory, comprises two circular sections (flanges) constructed from tape springs, joined along a longitudinal edge (web). Recently, various investigations have been conducted on composite TRAC booms due to the observed thermal gradient challenges associated with metallic booms in solar sail applications [? ]. Murphey and Banik [? ] stated that the best stacking sequence is  $[0^\circ, \pm 45^\circ, 0^\circ]$  for each circular boom flange, where  $0^\circ$  is the longitudinal

direction of the structure.

The core operational objectives for deployable studies are twofold: first, they must fold to minimize the overall volume in the stowed configuration and deploy in orbit to achieve the intended deployed configuration [? ]. Hence, a computational tool capable of simulating the deployment behavior proves invaluable for conducting sensitivity analyses and reducing the scope of the required experimental testing. The prevalent method for numerically analyzing such structures is the finite element method. However, traditional two-dimensional finite elements available in widely utilized commercial software must satisfy specific aspect-ratio constraints, which pose significant challenges primarily because of the slender nature of the structure. This approach, however, precludes the determination of out-of-plane effects exhibited by composite materials [? ? ? ], thus preventing the capture of local phenomena.

The solution proposed in the present research relies on a finite element mathematical model constructed within the framework of the Carrera Unified Formulation (CUF) [? ]. CUF enables the creation of 1D models with enhanced cross-sectional capabilities through the utilization of higher-order expansion functions. Consequently, it becomes possible to capture three-dimensional (3D) and localized effects [? ]. Furthermore, CUF has the capability of developing mathematical models requiring fewer degrees of freedom in comparison to conventional finite elements. This capability is achieved through the utilization of higher-order polynomials to approximate cross-sectional displacements. Consequently, it becomes feasible to circumvent the aspect-ratio constraints of traditional 2D and 3D finite elements, especially in the case of composite materials [? ? ]. The efficiency and effectiveness of CUF models in assessing the buckling and post-buckling behavior of deployable structures have already been demonstrated [? ? ? ]. Moreover, an innovative global/local approach for the failure onset analysis of deployable composite thin and ultra-thin structures was developed [? ].

The formulation is here used to simulate the folding of ultra-thin longerons. For this purpose, an implicit simulation scheme is employed. This choice is particularly critical because the problem includes contact nonlinearities, which significantly increase its complexity. In many standard finite element formulations, these complexities often necessitate the use of explicit schemes, making it difficult to confidently verify the accuracy of the results. By contrast, the proposed approach leverages a quasi-static formulation, in which the nonlinear governing equations are solved iteratively using a Newton–Raphson linearization procedure under displacement control. This not only enables the precise modeling of contact interactions but also ensures numerical stability and reliability of the final solution. Furthermore, because the proposed enhanced finite elements are not constrained by strict aspect-ratios, they enable efficient modeling of significantly longer components. In this work, this capability is demonstrated by analyzing deployable structures measuring 1 m and 5 m in length. This approach not only circumvents the high computational costs typically associated with standard finite elements for large-scale problems but also maintains numerical accuracy and stability, making it especially suited for the study of deployable and long-span structural systems.

The layout of this paper is as follows. (i) Section II presents the proposed mathematical model for ultra-thin longerons

and details the modeling methods adopted for the cross-sectional approximation. (ii) Next, the nonlinear governing equations using the principle of virtual work and the contact model is formulated in Section III. (iii) Section ?? presents the key findings, which include the folding of a single 400 mm-long longeron and the analysis of much longer deployable structures formed by two longerons connected by transverse straight battens. Finally, the main conclusions are drawn.

## II. Refined one-dimensional finite element formulation of a longeron

The specific deployable structure that is analyzed is shown in Fig. 1. It is a foldable Triangular Rollable and Collapsible (TRAC) longeron.

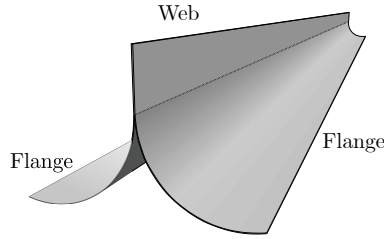


**Fig. 1 TRAC longeron. The curved domains are the flanges, the straight domain is the web.**

For the development of the numerical model, a Cartesian reference system is used, so that the  $y$ -direction is placed in the length direction, and the  $x, z$  coordinates identify the cross-sectional domain as shown in Fig. 2.

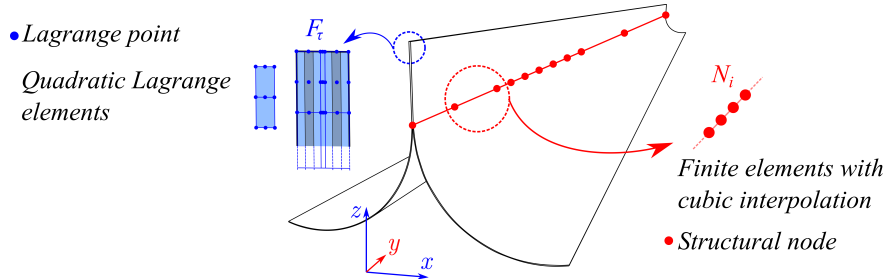


**Fig. 2 Model of TRAC longeron based on CUF.**

According to the Carrera Unified Formulation (CUF), the three-dimensional displacement field and its virtual variation can be written in the following unified manner:

$$\begin{aligned} \mathbf{u}(x, y, z) &= F_\tau(x, z)\mathbf{u}_\tau(y), \quad \tau = 1, 2, \dots, M \\ \delta\mathbf{u}(x, y, z) &= F_s(x, z)\delta\mathbf{u}_s(y), \quad s = 1, 2, \dots, M \end{aligned} \quad (1)$$

where  $F_\tau$  and  $F_s$  represent the cross-sectional functions depending on the  $x, z$  coordinate,  $\tau$  and  $s$  are the sum index and  $M$  is the number of terms of the expansion in the cross-section plane assumed for the displacements. The proposed work adopts quadratic Lagrange polynomials (L9) as  $F_\tau$  to approximate the kinematics. In this manner, higher-order

models can be implemented with ease (see Carrera and Petrolo [?] for more details). As an example, the displacement field evaluated through one L9 polynomial is quadratic and reads:

$$\begin{aligned}
u_x(x, y, z) &= F_1(x, z)u_{x_1}(y) + F_2(x, z)u_{x_2}(y) + \cdots + F_9(x, z)u_{x_9}(y) \\
u_y(x, y, z) &= F_1(x, z)u_{y_1}(y) + F_2(x, z)u_{y_2}(y) + \cdots + F_9(x, z)u_{y_9}(y) \\
u_z(x, y, z) &= F_1(x, z)u_{z_1}(y) + F_2(x, z)u_{z_2}(y) + \cdots + F_9(x, z)u_{z_9}(y)
\end{aligned} \tag{2}$$

where  $u_{x_1} \cdots u_{x_9}$  are the displacements of the points of the cross-sectional elements and  $F_1$  to  $F_9$  are functions of the cross-sectional coordinates. More details about the Lagrange expansion are described in [?]. To approximate the displacement field over the beam axis, the Finite Element Method (FEM) is adopted. The generalized displacement vector  $\mathbf{u}_\tau(y)$  and the generalized variations  $\delta\mathbf{u}_s(y)$  are approximated as follows:

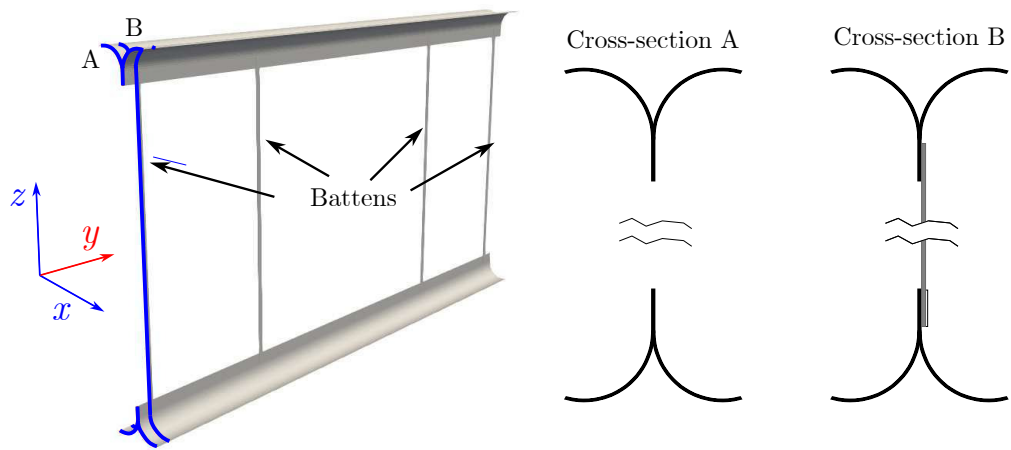
$$\begin{aligned}
\mathbf{u}_\tau(y) &= N_i(y)\mathbf{u}_{\tau i}, \quad i = 1, 2, \dots, N_n \\
\delta\mathbf{u}_s(y) &= N_j(y)\delta\mathbf{u}_{s j}, \quad j = 1, 2, \dots, N_n
\end{aligned} \tag{3}$$

where  $N_i$  and  $N_j$  stands for the  $i$ th one-dimensional shape function,  $i$  and  $j$  indicate summation and  $N_n$  is the number of the nodes per element. In the present work, linear (B2) and cubic (B4) elements are used.  $\mathbf{u}_{\tau i}$  and  $\delta\mathbf{u}_{s j}$  are the following vectors of the FE nodal parameters:

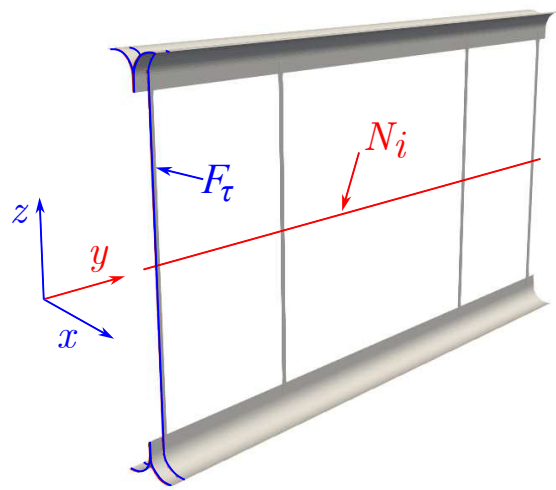
$$\begin{aligned}
\mathbf{u}_{\tau i} &= \{\mathbf{u}_{x\tau i} \ \mathbf{u}_{y\tau i} \ \mathbf{u}_{z\tau i}\}^T \\
\delta\mathbf{u}_{s j} &= \{\delta\mathbf{u}_{x s j} \ \delta\mathbf{u}_{y s j} \ \delta\mathbf{u}_{z s j}\}^T
\end{aligned} \tag{4}$$

The current research makes use of classical 1D finite Lagrangian elements with four nodes which provide a cubic interpolation along the  $y$  axis. See [?] for more details about these interpolations. Figure 2 shows the resulting one-dimensional model of the TRAC longeron.

Another deployable structures analyzed in this work is representes by a combination of two TRAC longerons connected by straight battens, building the *so-called* strip. Exploiting the capabilities of CUF, the complicated geometry is modeled using a single beam whose axis is along the  $y$ -direction, and the cross-sections are in  $x, z$  plane. Two cross-sections are defined using Lagrange elements, one including the battens and one without the battens. They alternate at the corresponding structural nodes to achieve the geometry of the total structure. Details of this approach are given in Fig. 3(a). The displacement field is then evaluated using  $N_i$  shape functions and  $F_\tau$  expansion functions over the axis and the cross-section, respectively, as reported in Fig. 3(b).



(a)



(b)

**Fig. 3** (a) Geometry of the proposed model of the strip. (b) Numerical model of the strip using CUF

### A. Strain field and constitutive relations

The stress,  $\sigma$ , and strain,  $\epsilon$ , components are expressed in vectorial form

$$\begin{aligned}\sigma &= \{\sigma_{xx} \ \sigma_{yy} \ \sigma_{zz} \ \sigma_{xz} \ \sigma_{yz} \ \sigma_{xy}\}^T \\ \epsilon &= \{\epsilon_{xx} \ \epsilon_{yy} \ \epsilon_{zz} \ \epsilon_{xz} \ \epsilon_{yz} \ \epsilon_{xy}\}^T\end{aligned}\tag{5}$$

As far as the strain field is concerned, the Green-Lagrange nonlinear strain components are

$$\epsilon = \epsilon_l + \epsilon_{nl} = (\mathbf{b}_l + \mathbf{b}_{nl})\mathbf{u},\tag{6}$$

where the  $6 \times 3$  linear and nonlinear differential operators  $\mathbf{b}_l$  and  $\mathbf{b}_{nl}$  are given by:

$$\mathbf{b}_l = \begin{bmatrix} \partial_x & 0 & 0 \\ 0 & \partial_y & 0 \\ 0 & 0 & \partial_z \\ \partial_z & 0 & \partial_x \\ 0 & \partial_z & \partial_y \\ \partial_y & \partial_x & 0 \end{bmatrix}, \quad \mathbf{b}_{nl} = \begin{bmatrix} \frac{1}{2}(\partial_x)^2 & \frac{1}{2}(\partial_x)^2 & \frac{1}{2}(\partial_x)^2 \\ \frac{1}{2}(\partial_y)^2 & \frac{1}{2}(\partial_y)^2 & \frac{1}{2}(\partial_y)^2 \\ \frac{1}{2}(\partial_z)^2 & \frac{1}{2}(\partial_z)^2 & \frac{1}{2}(\partial_z)^2 \\ \partial_x \partial_z & \partial_x \partial_z & \partial_x \partial_z \\ \partial_y \partial_z & \partial_y \partial_z & \partial_y \partial_z \\ \partial_x \partial_y & \partial_x \partial_y & \partial_x \partial_y \end{bmatrix}\tag{7}$$

in which  $\partial_\alpha = \partial(\cdot)/\partial\alpha$ ,  $\partial_\beta = \partial(\cdot)/\partial\beta$ , and  $\partial_z = \partial(\cdot)/\partial z$ . For the constitutive relation, linear elastic isotropic shell structures are considered in this work. Consequently, the constitutive relation reads as:

$$\sigma = \mathbf{C}\epsilon\tag{8}$$

where  $C$  is the material elastic matrix [? ?]. Finally, introducing the CUF and FEM (Eq. (3)) relations into Eq. (6), the strain vector can be written in algebraic form as follows:

$$\boldsymbol{\epsilon} = (\mathbf{B}_l^{\tau i} + \mathbf{B}_{nl}^{\tau i}) \mathbf{q}_{\tau i} \quad (9)$$

where  $\mathbf{B}_l^{sj}$  and  $\mathbf{B}_{nl}^{sj}$  are the linear and nonlinear algebraic matrices with CUF and FEM formulations. The explicit form of these two matrices are not reported here for the sake of brevity, but they are reported in [? ].

### III. Nonlinear governing equations

The derivation of the nonlinear governing equations is described in [? ] and is briefly summarized here. The principle of virtual displacements can be written as

$$\delta L_{\text{int}} = \delta L_{\text{ext}} \quad (10)$$

where  $\delta L_{\text{int}}$  and  $\delta L_{\text{ext}}$  are the virtual variations of the internal strain energy and the external work, respectively, with  $\delta$  denoting the variation. The virtual variation of the internal strain energy for a body of volume  $V$  can be expressed as:

$$\delta L_{\text{int}} = \int_V \delta \boldsymbol{\epsilon}^T \boldsymbol{\sigma} \, dV \quad (11)$$

and

$$\delta \boldsymbol{\epsilon} = \delta((\mathbf{B}_l^{sj} + \mathbf{B}_{nl}^{sj}) \mathbf{q}_{sj}) = \delta \mathbf{q}_{sj}^T (\mathbf{B}_l^{sj} + 2\mathbf{B}_{nl}^{sj}) \quad (12)$$

Introducing Eq. (12) into Eq. (11), gives

$$\begin{aligned}
\delta L_{\text{int}} &= \delta \mathbf{q}_{sj}^T \int_V (\mathbf{B}_l^{sj} + 2\mathbf{B}_{nl}^{sj})^T \boldsymbol{\sigma} \, dV = \\
&= \delta \mathbf{q}_{sj}^T \int_V (\mathbf{B}_l^{sj} + 2\mathbf{B}_{nl}^{sj})^T \mathbf{C} (\mathbf{B}_l^{\tau i} + \mathbf{B}_{nl}^{\tau i}) \, dV \mathbf{q}_{\tau i} = \\
&= \delta \mathbf{q}_{sj}^T \mathbf{K}_0^{ij\tau s} \mathbf{q}_{\tau i} + \delta \mathbf{q}_{sj}^T \mathbf{K}_{lnl}^{ij\tau s} \mathbf{q}_{\tau i} \\
&+ \delta \mathbf{q}_{sj}^T \mathbf{K}_{nll}^{ij\tau s} \mathbf{q}_{\tau i} + \delta \mathbf{q}_{sj}^T \mathbf{K}_{nlnl}^{ij\tau s} \mathbf{q}_{\tau i} \\
&= \delta \mathbf{q}_{sj}^T \mathbf{K}_S^{ij\tau s} \mathbf{q}_{\tau i}
\end{aligned} \tag{13}$$

where  $\mathbf{K}_S^{ij\tau s} = \mathbf{K}_0^{ij\tau s} + \mathbf{K}_{lnl}^{ij\tau s} + \mathbf{K}_{nll}^{ij\tau s} + \mathbf{K}_{nlnl}^{ij\tau s}$  represents the *so-called* fundamental nucleus of the secant stiffness matrix. These are  $3 \times 3$  matrices that, given the cross-sectional ( $F_\tau$  and  $F_s$ ) and shape ( $N_i$  and  $N_j$ ) functions, can be expanded by looping on the indexes  $\tau, s = 1, 2, \dots, M$ , and  $i, j = 1, \dots, N_n$  in order to obtain the elemental secant stiffness matrix. After obtaining the elemental secant stiffness matrix, it can be assembled using the conventional FEM approach (see [? ]).

In Eq. (13),  $\mathbf{K}_0^{ij\tau s}$ ,  $\mathbf{K}_{lnl}^{ij\tau s}$ ,  $\mathbf{K}_{nll}^{ij\tau s}$ , and  $\mathbf{K}_{nlnl}^{ij\tau s}$  constitute the linear and nonlinear constituents of  $\mathbf{K}_S^{ij\tau s}$ . Their expressions are as follows:

$$\begin{aligned}
\mathbf{K}_0^{ij\tau s} &= \int_V (\mathbf{B}_l^{sj})^T \mathbf{C} \mathbf{B}_l^{\tau i} \, dV & \mathbf{K}_{lnl}^{ij\tau s} &= \int_V (\mathbf{B}_l^{sj})^T \mathbf{C} \mathbf{B}_{nl}^{\tau i} \, dV \\
\mathbf{K}_{nll}^{ij\tau s} &= 2 \int_V (\mathbf{B}_{nl}^{sj})^T \mathbf{C} \mathbf{B}_l^{\tau i} \, dV & \mathbf{K}_{nlnl}^{ij\tau s} &= 2 \int_V (\mathbf{B}_{nl}^{sj})^T \mathbf{C} \mathbf{B}_{nl}^{\tau i} \, dV
\end{aligned} \tag{14}$$

It is important to note that the  $\mathbf{K}_S$  matrix described above, is non-symmetric, which can lead to both mathematical and practical limitations. The authors have sought solutions to address these issues by investigating innovative approaches to formulate symmetric versions of the secant stiffness matrix for a broader range of problems (see, for instance, [? ? ? ]). In the present study, the same symmetric representation of the secant stiffness matrix as described in [? ] is established,

by describing the virtual variation in internal strain energy attributed to the contribution  $\mathbf{K}_{nll}^{ij\tau s}$  in the following manner:

$$\begin{aligned}
\delta L_{\text{int}nll} &= \int_V \delta \boldsymbol{\epsilon}^T \boldsymbol{\sigma} \, dV \\
&= \frac{1}{2} \int_V \delta \boldsymbol{\epsilon}_{nl}^T \mathbf{C} \boldsymbol{\epsilon}_l + \delta \boldsymbol{\epsilon}_{nl}^T \boldsymbol{\sigma}_l \, dV \\
&= \delta \mathbf{q}_{sj}^T (\mathbf{K}_{nll}^{ij\tau s} + \mathbf{K}_{\sigma l}^{ij\tau s}) \mathbf{q}_{\tau i}
\end{aligned} \tag{15}$$

Hence, in accordance with Eq. (13), the complete virtual variation of the strain energy is as follows:

$$\delta L_{\text{int}} = \delta \mathbf{q}_{sj}^T (\mathbf{K}_0^{ij\tau s} + \mathbf{K}_{lnl}^{ij\tau s} + \frac{1}{2} \mathbf{K}_{nll}^{ij\tau s} + \frac{1}{2} \mathbf{K}_{\sigma l}^{ij\tau s} + \mathbf{K}_{nlnl}^{ij\tau s}) \mathbf{q}_{\tau i} \tag{16}$$

The expansion of the fundamental nucleus of the secant stiffness matrix has now yielded a symmetric form.

On the other hand, the expression of the external load vector is computed from the definition of the virtual variation of the work made by external forces. Omitting some mathematical derivations, it can be written as

$$\delta L_{\text{int}} = \delta \mathbf{q}_{sj}^T \mathbf{F}_{ext}^{\tau i} \tag{17}$$

Finally, the fully assembled stiffness matrix and force vector are obtained by looping the index  $i$ ,  $j$ ,  $\tau$  and  $s$  in the fundamental nucleus of Eq. (16) and the index  $\tau$  and  $i$  in the fundamental nucleus of Eq. (17). As a result, introducing the results in Eq. (10), the following nonlinear equation holds

$$\mathbf{K}_S \mathbf{q} = \mathbf{F}_{ext} \tag{18}$$

Equation (18) represents a geometrically nonlinear systems, and is typically computed adopting a linearization technique. In this paper, the employed linearization technique is the Newton-Raphson method, according to which, the nonlinear governing equations are expressed as

$$\boldsymbol{\varphi}_{res} \equiv \mathbf{K}_S \mathbf{q} - \mathbf{F}_{ext} = 0 \tag{19}$$

where the *residual nodal forces* vector is denoted by  $\boldsymbol{\varphi}_{res}$ . A known  $(\mathbf{q}, \mathbf{p})$  solution can be used to linearize Eq. (19) by expanding  $\boldsymbol{\varphi}_{res}$  in a Taylor's series. Therefore,

$$\boldsymbol{\varphi}_{res}(\mathbf{q} + \delta \mathbf{q}, \mathbf{p} + \delta \mathbf{p}) = \boldsymbol{\varphi}_{res}(\mathbf{q}, \mathbf{p}) + \frac{\partial \boldsymbol{\varphi}_{res}}{\partial \mathbf{q}} \delta \mathbf{q} + \frac{\partial \boldsymbol{\varphi}_{res}}{\partial \mathbf{p}} \delta \mathbf{p} = 0 \tag{20}$$

where  $\frac{\partial \boldsymbol{\varphi}_{res}}{\partial \mathbf{q}} = \mathbf{K}_T$  represents the *tangent* stiffness matrix.

The external load is expressed in terms of a reference load  $\mathbf{p}_{ref}$  and a load-scaling parameter  $\lambda$ , i.e.  $\mathbf{p} = \lambda \mathbf{p}_{ref}$ . Since  $\lambda$  is a variable, an additional equation is required, and this is given by a relation involving both  $\delta \mathbf{q}$  and  $\delta \lambda$ . Finally, it can be written

$$\begin{cases} \mathbf{K}_T \delta \mathbf{q} = \delta \lambda \mathbf{p}_{ref} - \boldsymbol{\varphi}_{res} \\ c(\delta \mathbf{q}, \delta \lambda) = 0 \end{cases} \quad (21)$$

In the current work, the condition  $c(\delta \mathbf{q}, \delta \lambda) = \delta \mathbf{q} = 0$  is considered, so that the displacement control method is employed. More details can be found in [? ? ?]. It is important to underline that  $\mathbf{K}_T$  is derived from the linearization of the equilibrium equations [?]. This corresponds to the linearization of the virtual variation of the work by the internal conservative forces, as follows

$$\delta(\delta L_{int}) = \int_V \delta(\delta \boldsymbol{\epsilon}^T \boldsymbol{\sigma}) dV = \delta \mathbf{q}_{sj}^T \mathbf{K}_T^{ij\tau s} \delta \mathbf{q}_{\tau i} \quad (22)$$

$\mathbf{K}_T^{ij\tau s}$  represents the fundamental nucleus of the tangent stiffness matrix [?].

### A. Contact mechanics

Contact between the flanges of the longeron is modeled as node-to-surface contact. Consider two generic bodies,  $\Omega_M$  and  $\Omega_S$ , as depicted in Fig. 4. It is convenient to identify one body as *master* and the other as *slave* [?], corresponding to  $\Omega_M$  and  $\Omega_S$ , respectively. At each point of the master body, it is possible to construct unit vectors tangent to the surface  $\mathbf{e}_M^1$  and  $\mathbf{e}_M^2$ , which are equal to  $\mathbf{e}_M^x$  and  $\mathbf{e}_M^y$ , according to a Cartesian reference system.

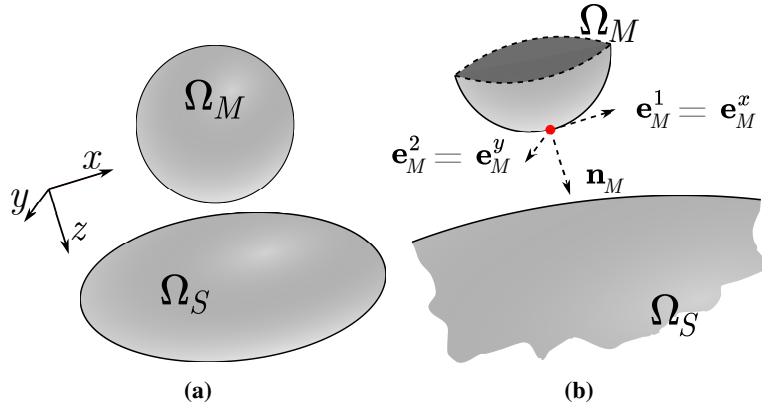


**Fig. 4** Generic bodies in contact and unit vectors of the master body.

The normal to body  $\Omega_M$  is given by

$$\mathbf{n}_M = \mathbf{e}_M^x \times \mathbf{e}_M^y \quad (23)$$

In a node-to-surface contact, each node of the master body is compared to the surface of the slave body. Figure 5 shows the distance vector  $\mathbf{d}$  between the master and the slave bodies, for a chosen point on the master body.

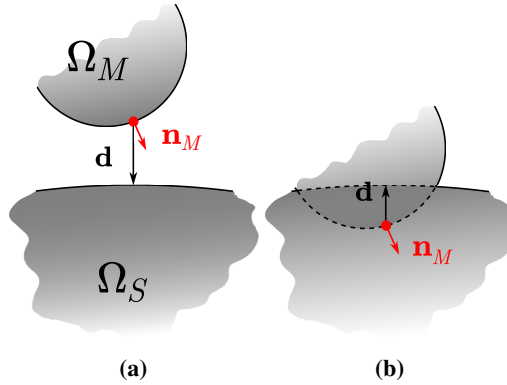


**Fig. 5 Distance vector  $\mathbf{d}$  between master and slave bodies.**

From a physical point of view, the bodies are in contact when they are close to interpenetrate. From a computational point of view, the contact activates when the scalar  $|\mathbf{d}|$  of distance vector  $\mathbf{d}$  is negative. It follows the following relation:

$$\left\{ \begin{array}{l} \text{if } \mathbf{d} \cdot \mathbf{n}_M > 0 \quad \Rightarrow \quad |\mathbf{d}| > 0 \\ \text{if } \mathbf{d} \cdot \mathbf{n}_M \leq 0 \quad \Rightarrow \quad |\mathbf{d}| \leq 0 \end{array} \right. \quad (24)$$

In the case of  $\mathbf{d} \cdot \mathbf{n}_M \leq 0$ , corresponding to Fig. 5(b), a spring is activated, which produces two opposite forces, as depicted in Fig. 6.

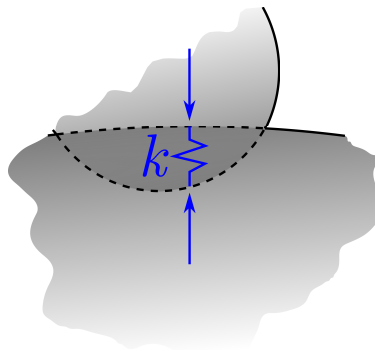


**Fig. 6 A spring is activated when the bodies interpenetrate.**

During the folding of the longeron, the two inner surfaces of the flanges come into contact, and the aforementioned contact mechanics are considered during the simulation. In this work, the surface laying in the positive  $x$ -axis is

considered as the slave, whereas the other surface is considered as the master, as depicted in Fig. 7.

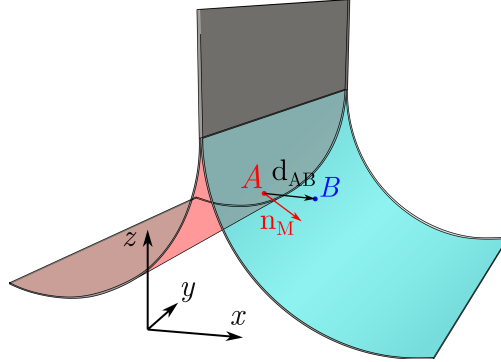


**Fig. 7 Master (red) and slave (blue) surfaces of the TRAC longeron for the contact simulation.**

For each point of the master surface, the normal vector  $\mathbf{n}_M$  is evaluated. Figure 7 also shows the vector  $\mathbf{d}_{AB}$  indicating the distance between the slave point and the closest point on the master surface. For the definition of the distance and, the interpenetration of the two nodes the same notation of [?] is used, so that

$$|\mathbf{d}_{AB}| = \|\mathbf{u}^B - \mathbf{u}^A\| = \|F_\tau N_i \mathbf{u}_{\tau i}^B - F_\tau N_i \mathbf{u}_{\tau i}^A\| = F_\tau N_i \|\mathbf{u}_{\tau i}^B - \mathbf{u}_{\tau i}^A\| \quad (25)$$

The sign of  $|\mathbf{d}_{AB}|$  is defined according to the following rule:

$$\left\{ \begin{array}{l} \text{if } (\mathbf{u}_{\tau i}^B - \mathbf{u}_{\tau i}^A) \cdot \mathbf{n}_{M \tau i} > 0 \quad \Rightarrow \quad |\mathbf{d}_{AB}| > 0 \\ \text{if } (\mathbf{u}_{\tau i}^B - \mathbf{u}_{\tau i}^A) \cdot \mathbf{n}_{M \tau i} \leq 0 \quad \Rightarrow \quad |\mathbf{d}_{AB}| \leq 0 \end{array} \right. \quad (26)$$

The virtual work due to the contact spring forces is defined as

$$\begin{aligned} \delta L_c &= \int_{dA} k \mathbf{d}_{AB} \delta \mathbf{d}_{AB}^T dA \\ &= \int_{dA} k F_\tau N_i \mathbf{u}_{\tau i}^B F_s N_j \delta \mathbf{u}_{s j}^{T B} dA - \int_{dA} k F_\tau N_i \mathbf{u}_{\tau i}^A F_s N_j \delta \mathbf{u}_{s j}^{T A} dA \\ &= \delta \mathbf{u}_{s j}^{T B} \mathbf{F}_c^{\tau i B} - \delta \mathbf{u}_{s j}^{T A} \mathbf{F}_c^{\tau i A} = \delta \mathbf{u}_{s j}^T \mathbf{F}_c^{\tau i} \end{aligned} \quad (27)$$

where  $dA$  is the contact surface. By looping on the indexes  $\tau$  and  $i$  the global contact force vector  $\mathbf{F}_c$  is evaluated. This

contact force term is added to the external force vector  $\mathbf{F}_{ext}$  of Eq. (18), and the resulting vector  $\bar{\mathbf{F}}$  is represented by

$$\bar{\mathbf{F}} = \mathbf{F}_c + \mathbf{F}_{ext} \quad (28)$$

The global contact penalty stiffness matrix  $\mathbf{K}_c$  is then formed by adding the contact terms, given by

$$\mathbf{k}^{\tau i} = k \mathbf{n}_{M\tau i}^T \mathbf{n}_{M\tau i} \quad (29)$$

The term  $\mathbf{K}^c$  is then added to  $\mathbf{K}^T$  in Eq. (22) to update the global stiffness matrix.